International Journal of GEOMATE, June, 2026 Vol.30, Issue 142, pp.21-31
ISSN: 2186-2982 (P), 2186-2990 (O), Japan, DOI: https://doi.org/10.21660/2026.142.5341
Geotechnique, Construction Materials and Environment

INTERPRETING LINEAMENTS USING REMOTE SENSING AND GIS ANALYSIS FOR PREDICTING CAVE DIRECTIONS: A CASE STUDY OF THAM SAI THONG CAVE AREA, CHIANG RAI, NORTHERN THAILAND

*Kiatsuradech Tansuwan[1] and Akkhapun Wannakomol[1]

[1]School of Geotechnology, Institute of Engineering, Suranaree University of Technology, Nakhon Ratchasima, 30000 Thailand

*Corresponding Author, Received: 18 Nov. 2026, Revised: 22 Feb. 2026, Accepted: 09 March 2026

ABSTRACT: This study presents a semi-automated geospatial approach for predicting subterranean pathway orientations in the Tham Sai Thong cave area, Chiang Rai, Northern Thailand. High-resolution Sentinel-2 imagery and a Digital Elevation Model (DEM) derived from the ALOS satellite were utilized to objectively extract geological lineaments. Their spatial correlation with karst depressions and surveyed cave entrances was analyzed to infer probable subsurface pathways. Preprocessing involved band stacking and Topographic Position Index (TPI) enhancement, while Canny edge detection followed by the Hough Transform facilitated efficient, semi-automated lineament extraction. Although the core extraction and overlay procedures are parameterized and reproducible, parameter calibration and final depression validation involve limited expert-guided refinement. Karst depressions were identified via DEM differential analysis (fill-sinks method) and validated against topographic and satellite data. Cave entrances, accurately surveyed by GNSS, were integrated with high-density lineament zones using spatial buffering and a Multiplicative Boolean Overlay (Map Algebra). Two dominant lineament orientations—NW-SE and NNE-SSW—were observed, consistent with the regional tectonic framework and interpreted principal stress orientation associated with the Mae Chan Fault system. The predicted cave directions demonstrated high accuracy, with spatial overlaps of 93.67% with Shepton Mallet Caving Club data and 81.47% with Department of Mineral Resources maps, demonstrating the practical utility of integrated GIS and remote sensing for structured cave direction prediction in structurally controlled karst terrains.

Keywords: Lineament, Cave, Hough transform, Karst feature, Limestone

1. INTRODUCTION

The geological complexity of karst terrains presents a significant challenge for geological surveying, infrastructure development, and geohazard management worldwide. These landscapes, formed by the dissolution of soluble rocks such as limestone and marble, are characterized by intricate subsurface drainage systems, sinkholes, and extensive cave networks. Their inherent anisotropy and heterogeneity make the prediction of subsurface features and groundwater flow paths exceptionally difficult. The 2018 rescue of the Moo Pa football team from Tham Luang Cave in Chiang Rai, Northern Thailand, highlighted the urgent need for detailed structural and geological information in emergency response situations [1]. Although satellite-derived 3D models were generated during the crisis by agencies including GISTDA [2], comprehensive structural datasets linking surface morphology to subsurface conduits remain limited. Cave development in the Nang Non Mountains is strongly influenced by regional tectonic structures, particularly the Mae Chan Fault, and by dissolution along pre-existing fractures within Permo–Carboniferous limestone and marble units [3].

Traditional acquisition of geological structural data in rugged karst terrain relies heavily on field surveys, which, although accurate, are time-consuming and often constrained by accessibility. Consequently, Remote Sensing (RS) and Geographic Information Systems (GIS) have become efficient tools for extracting structural information through lineament interpretation [4]. Lineaments—observable linear surface features reflecting geological discontinuities [5, 6]—appear in satellite imagery as tonal contrasts, textural alignments, or topographic breaks influenced by vegetation and moisture patterns [7].

Methodologies for lineament extraction have progressively evolved from manual interpretation toward automated and semi-automated approaches. Reviews by Ahmadi and Pekkan (2021) emphasize the integration of multi-source remote sensing data to enhance detection reliability [8]. Edge detection techniques such as Canny and transform-based approaches such as the Hough Transform are widely applied to DEM and optical imagery [9, 10]. Integration of optical and DEM datasets has been shown to improve structural interpretation compared to single-source analysis [11]. In tropical environments, L-band SAR datasets such as ALOS

PALSAR have demonstrated advantages in structural detection beneath vegetation cover [12]. Recent developments further integrate GIS workflows with computational approaches to improve geohazard assessment efficiency [13].

The application of these geospatial techniques is particularly relevant to karst systems, where surface lineaments often correspond to zones of structural weakness influencing subsurface permeability. Nevertheless, surface lineaments represent two-dimensional geomorphic expressions of fracture and fault zones, whereas cave conduits develop as three-dimensional, hydraulically selective pathways within the rock mass. In tropical karst terrains, dense vegetation cover and intense weathering may further obscure direct surface–subsurface correspondence. Therefore, in the present study, lineaments are interpreted as structural proxies indicating preferential fracture orientations and potential zones of enhanced permeability rather than as direct spatial representations of individual cave passages. Lineament density analysis has been used to identify structurally controlled permeability zones in geothermal contexts [14], and GIS-based geomorphological integration has demonstrated reliability in mapping structural continuity [15].

However, landscape heterogeneity in subtropical and tropical karst regions complicates surface interpretation [16], even though multi-variable GIS workflows can effectively delineate karst features [17]. Broader GIS applications in hazard mitigation [18] and radar-based ground stability monitoring [19] further support the applicability of remote sensing in structurally complex terrains.

Synthesizing these developments, the geological principles linking surface lineaments to subsurface fractures—validated in recent structural and hazard mapping studies [20, 21]—are directly relevant to speleogenesis. However, despite technological progress, a specific gap remains in applying semi-automated lineament extraction workflows to predict subterranean cave pathways in tropical karst environments. Most existing studies emphasize regional tectonic mapping or generalized susceptibility assessment without establishing directional relationships to mapped cave systems or validating results against independent speleological surveys.

Unlike most GIS-based karst investigations, which focus primarily on structural delineation or surface susceptibility mapping, the present study integrates morphometric DEM enhancement, semi-automated Hough Transform lineament extraction, density-guided structural refinement, and probabilistic cave-direction modeling within a unified geospatial framework. Furthermore, predicted structural trends are evaluated against independent speleological survey data, thereby extending analysis beyond surface feature identification toward directional validation of subsurface cave pathways.

This study addresses this gap by proposing a semi-automated geospatial approach to predict cave directions in the Tham Sai Thong cave area, part of the Tham Luang–Khun Nam Nang Non cave system. The methodology employs Topographic Position Index (TPI) enhancement on ALOS DEMs to highlight subtle topographic breaks, followed by objective lineament extraction using the Hough Transform algorithm. These features are integrated with karst depressions through a Multiplicative Boolean Overlay to model probable subsurface pathways.

The primary aim of this research is to analyze fracture structures in the study area using lineament interpretation integrated with geospatial analysis to predict probable subsurface cave directions. Specifically, the objectives are: (1) to detect potential cave-forming lineaments using semi-automated Hough Transform extraction on TPI-enhanced DEM; and (2) to validate predicted cave orientations using geological and speleological survey data.

The remainder of this paper is organized as follows: Section 2 outlines the research significance. Section 3 details the materials and the integrated GIS methodology. Section 4 presents the results of the lineament analysis and validates the predicted cave directions against field survey maps. Finally, Section 5 concludes the study and discusses the implications for future karst exploration.

2. RESEARCH SIGNIFICANCE

Drawing lessons from the 2018 Tham Luang crisis, this research proposes a semi-automated geospatial framework to predict subterranean cave pathways in the Tham Sai Thong area. By integrating Topographic Position Index (TPI) enhancement with the Hough Transform and a Multiplicative Boolean Overlay, the study offers a novel, objective alternative to subjective manual interpretation. This methodology enables rapid, cost-effective modeling of subterranean environments. Its primary significance lies in providing a reproducible predictive mapping tool and a framework applicable to geohazard assessment, resource exploration, and emergency response planning in complex, structurally controlled karst terrains.

3. MATERIAL AND METHODS

3.1 Study Area

The Tham Sai Thong cave area is located within the Tham Luang–Khun Nam Nang Non National Park in Chiang Rai Province, Northern Thailand (UTM coordinates: 590925E, 2252910N) [22] (Fig.1). Geologically, the area forms part of the Permo-Carboniferous sedimentary and metamorphic belt,

with the CP3-2 marble unit as the dominant lithology. This carbonate unit is highly susceptible to karstification and exhibits fracture systems influenced by the broader tectonic regime of the Mae Chan Fault (regional context) [23]. Although the principal fault trace does not directly intersect the study area, regional tectonic stresses have contributed to the development of local structural discontinuities. The regional structural framework and interpreted principal stress orientation are illustrated in Fig.2.

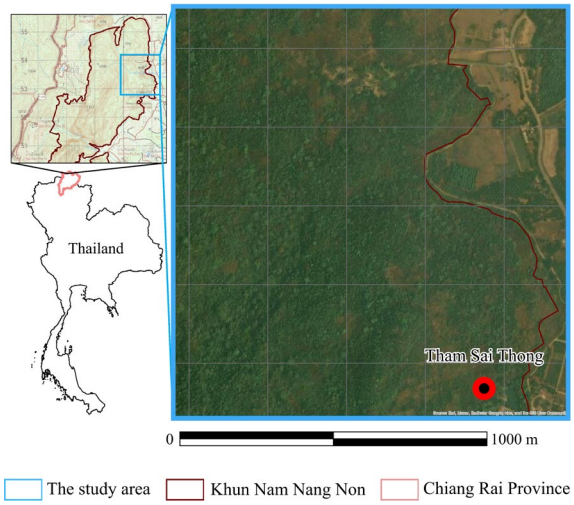

Fig.1 Location of the Tham Luang–Khun Nam Nang Non National Park, Chiang Rai Province, Northern Thailand.

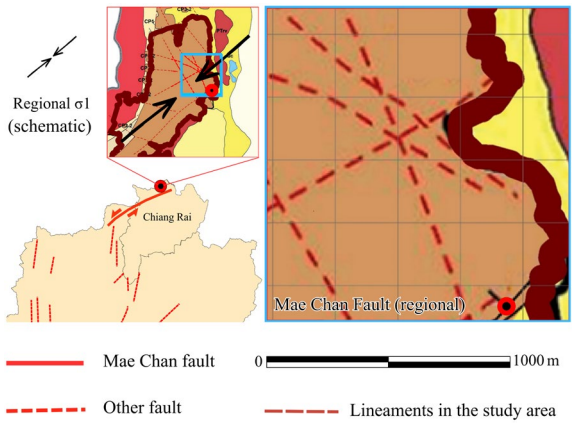

Fig.2 Regional structural framework showing the Mae Chan Fault (regional), interpreted principal stress direction (σ1), and regional fault influence on the study area.

The study area is characterized by dense tropical forest cover, which limits direct structural interpretation from optical satellite imagery due to reduced bedrock exposure. Consequently, radar-based data and DEM-derived morphometric analysis provide a more reliable means of identifying structural controls beneath vegetation.

The structural orientation context for the study area is supported by the geological mapping conducted by Bunchaiwong et al. [23], which is based on field investigations and regional structural analysis. The official DMR structural map and related geological interpretations, therefore, provide field-derived reference orientations against which the remotely extracted lineaments are evaluated. The present study focuses on morphometric and geospatial extraction rather than conducting new scan-line fracture measurements, and validation is performed through comparison with these established geological datasets.

3.2 Data

Two primary remote sensing datasets were utilized to establish the geospatial foundation of this study. The first dataset, Sentinel-2 satellite imagery, was acquired from the Copernicus Open Access Hub [24], providing 13 spectral bands from which specific bands (2, 3, 4, 8, 11, and 12) were selected for detailed surface feature analysis. In addition to true-color composites (Bands 2–4), Band 8 (NIR) and Bands 11–12 (SWIR) were examined to assess vegetation cover and surface moisture variations in relation to topographic features. These bands provided supplementary visual support for identifying geomorphic expressions potentially associated with structural discontinuities.

However, due to spatial resolution constraints, detailed fracture-scale moisture detection was limited; therefore, Sentinel-2 imagery was primarily used for contextual validation, while DEM-derived morphometric analysis served as the principal basis for lineament extraction.

Complementing this, an ALOS PALSAR Digital Elevation Model (DEM) was obtained from the Alaska Satellite Facility (ASF) [25]. This L-band Synthetic Aperture Radar (SAR) data, featuring a high spatial resolution of 12.5 meters, served as the critical baseline for the subsequent topographic and hydrological analyses essential for lineament extraction. The ALOS PALSAR DEM was selected due to its L-band radar acquisition, which enhances structural surface detection under vegetated conditions. The 12.5 m spatial resolution is appropriate for regional-scale fracture analysis while maintaining consistency with the study area extent. Alternative freely available global DEM datasets provide comparatively coarser resolution, which may be less suitable for detailed structural interpretation at this scale. The use of openly accessible DEM data also supports methodological reproducibility.

3.3 Research methodology

The study employed a four-stage geospatial framework: (1) Data Preprocessing, (2) Semi-

automated Lineament Extraction, (3) Karst Depression Analysis, and (4) Cave Direction Prediction Modeling. All spatial processing and model implementation were conducted in ArcMap version 10.8.1 (Esri), with parameter settings explicitly defined in the respective subsections to ensure methodological reproducibility.

3.3.1 Data preprocessing

Preprocessing involved layer stacking of the selected Sentinel-2 bands to enhance visual interpretation. Crucially, the Topographic Position Index (TPI) was calculated from the ALOS DEM. A 7x7 pixel kernel matrix was empirically selected for this calculation. This specific kernel size proved to be the most effective scale for capturing intermediate-scale regional structural features and morphological breaks, ensuring an optimal balance between micro-scale noise suppression and macro-scale generalization [26]. The resulting TPI layer was essential for highlighting morpho-structural features relevant to fracture patterns.

3.3.2 Semi-automated Lineament Extraction

To minimize subjective bias, lineaments were extracted using a semi-automated approach combining the Canny edge detection algorithm with the Hough Transform. The TPI images were first converted to 8-bit format for computational efficiency [27].

Parameter optimization was conducted through iterative testing within predefined ranges derived from established literature [28, 29]. For the Gaussian filter (Sigma), seven values ranging from 2.1 to 2.7 (at 0.1 increments) were evaluated to assess the trade-off between noise suppression and edge preservation. Lower Sigma values resulted in excessive pixel-level noise, whereas higher values reduced the visibility of minor structural edges. Visual coherence was used as the primary evaluation criterion, focusing on the clarity of structural boundaries and the minimization of spurious noise pixels. Based on this structured evaluation, a Sigma value of 2.4 provided the most stable balance for subsequent lineament extraction [30].

The threshold parameter in the Hough accumulator was similarly assessed through trial iterations to determine the minimum vote count required to isolate geologically meaningful lineaments while suppressing background noise [31]. A threshold of 12 yielded the clearest separation between structural features and random edges. Furthermore, a Minimum Line Length of 4 pixels was adopted to retain minor fractures relevant to karst morphology, and a Maximum Line Gap of 7 pixels was selected to connect collinear segments without excessive over-aggregation.

3.3.3 Karst depressions

Karst depressions, indicative of vertical recharge zones, were identified using a DEM differential analysis (fill-sinks technique). This method isolated negative elevation differences by comparing the filled DEM with the original unfilled DEM. The identified potential depressions were then validated through visual cross-referencing with Sentinel-2 imagery and topographic maps to filter out non-karst artifacts.

3.3.4 Cave direction prediction (Integrated GIS Model)

The prediction of cave directions was conducted through a four-step geospatial analysis framework that integrated field survey data with remote sensing derivatives.

Initially, the cave entrance location was determined via GNSS field surveys. To account for positional uncertainty, a 50-meter buffer was applied, a distance equivalent to twice the estimated GNSS error [32].

Concurrently, lineament density was analyzed using a 50-meter search radius, calculated by multiplying the minimum line length (4 pixels) by the 12.5-meter pixel resolution. This approach adheres to the Optimum Legible Delineation (OLD) criteria, which defines the minimum mappable unit as four times the pixel size to ensure visual clarity [33].

Subsequently, three significant karst depressions were buffered at 500 meters, corresponding to the standard 1:50,000 topographic map scale used to facilitate accurate geomorphological interpretation [34]. These depressions were grouped by spatial proximity and linked to the cave entrance using lineament density as a guiding parameter; the resulting connection lines were similarly buffered at 50 meters, consistent with OLD standards.

Finally, these spatial variables—cave entrance, lineament density, and karst depressions—were integrated using a Multiplicative Boolean Overlay in ArcMap. A scoring system was employed where absent features were assigned a neutral value of 1, while detected features were assigned values greater than 1 to amplify the composite score. The resulting probability raster was classified into five ordinal categories (Very Low to Very High) using the Jenks Natural Breaks method, a technique selected to maximize within-class homogeneity and between-class distinction [35, 36].

4. RESULT AND DISCUSSION

4.1 Topographic Position Index Image and Interpretation

The Topographic Position Index (TPI) was derived from ALOS DEMs using a 7×7 matrix, a parameter selected for its ability to accurately capture terrain structure while preserving the original pixel size [26]. Raster TPI images were generated via the focal statistics tool in ArcGIS, yielding values ranging from −21.47 to 19.80. These results were visualized using grayscale and color gradients to distinguish morphological features: low values (green) indicate depressions such as valleys or fractures; mid-range values (yellow) represent relatively flat areas like plains or water bodies; and high values (red) denote elevated features such as peaks, ridges, or hills. These interpretations were rigorously validated against topographic maps and Sentinel-2 imagery (Fig.3), facilitating the precise identification of morphologies significant for karst development.

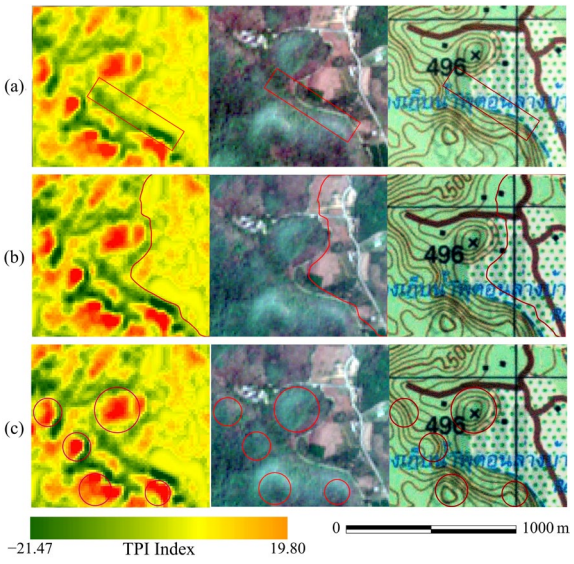

Fig.3 TPI image and corresponding satellite and topographic maps illustrating representative geomorphic features: (a) valley and cliffs, (b) plain area, and (c) ridge or hill.

4.2 Lineament Detection

For computational efficiency, TPI images were converted to 8-bit TIFF format. The lineament detection was performed using the semi-automated Hough Transform with the optimized parameters detailed in Section 3.3.2. This approach balanced noise suppression with the preservation of significant edge features relevant to karst morphology, ensuring the objective extraction of potential structural lineaments from the terrain data.

4.3 Lineament Density and Orientation

Lineament density was analyzed with a 50-meter search radius, consistent with the scale of the official DMR structural map [37]. The "Pre-Line" dataset (initial extraction) identified 151 lineaments with an average length of 201.13 m, as visualized in the density image (Fig.4). Following spatial aggregation, the "Post-Line" dataset was refined to 31 lineaments (Table 1).

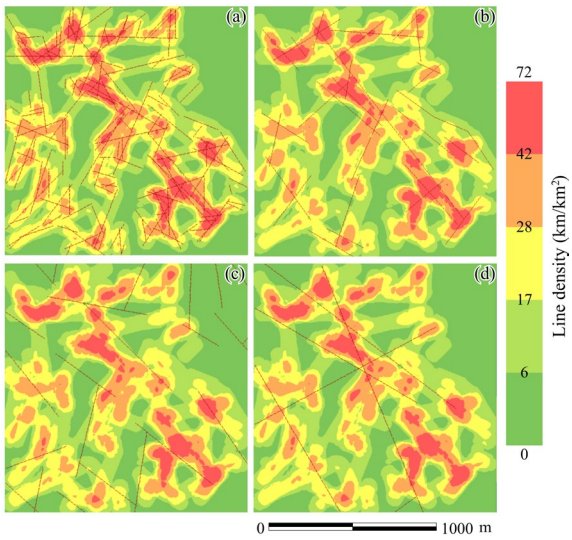

Fig.4 Lineament density maps with overlaid structural features: (a) Pre-line dataset, (b) Post-line dataset, (c) Lineament structure map, and (d) Geological map from DMR [37].

Table 1. Number, maximum, minimum, and mean of lineaments for each data.

Name	Number of lineaments	Max	Min	Mean
a	151	663.9	50.56	201.13
b	31	1340	123	343.94
c	23	689	116	356.00
d	7	1484	176	879.857

a is Pre-line, b is Post-line, c is Lineament structure map, d is Geological map [37]

The refinement from the Pre-Line to the Post-Line dataset involved a density-guided cartographic generalization step. The initial Hough-based extraction produced fragmented segments representing localized morphometric discontinuities. To obtain structurally meaningful lineaments suitable for regional interpretation, manual re-digitization was performed using the ArcGIS Editor tool. Two explicit criteria were applied: (i) only lineaments with a minimum length of 100 m were retained to maintain consistency with the effective mapping scale, 10 times the 1:10,000 DMR structural map; and (ii)

digitization was guided by zones of spatially coherent lineament density, where raw segments exhibited directional clustering and spatial continuity. The procedure was visually evaluated and independently cross-checked by the co-author. Orientation agreement with the DMR structural map was assessed qualitatively; however, no geometric forcing or positional matching was imposed. It should be noted that the DMR map represents expert-based cartographic interpretation at a 1:10,000 scale, whereas the present extraction is derived from pixel-based morphometric analysis at 12.5 m spatial resolution. Consequently, the comparison emphasizes consistency in structural orientation trends rather than strict geometric correspondence between individual line segments.

Crucially, the Post-Line features exhibited an increased average length of 343.94 m, aligning closely with the 356.00 m average recorded in the official Lineament Structure Map by the Department of Mineral Resources (DMR) [37]. The density distribution across length intervals is detailed in Table 2. Orientation analysis via rose diagrams (Fig.5) revealed dominant trends in the NW-SE and NNE-SSW directions, which are consistent with the regional tectonic structures influenced by the Mae Chan Fault. Importantly, the dominant NW–SE and NNE–SSW modes remain stable before and after filtering, indicating that the reduction primarily removes subordinate and spurious orientations rather than reshaping the main structural trends.

Table 2. Density values of lineaments across different length intervals.

Lineament range (m)	a	b	c	d
<100	35 (23.18%)	0 (0.00%)	0 (0.00%)	0 (0.00%)
100-200	65 (43.05%)	3 (9.68%)	3 (13.04%)	1 (14.29%)
200-300	22 (14.57%)	14 (45.16%)	8 (34.78%)	0 (0.00%)
300-400	12 (7.95%)	6 (19.35%)	3 (13.04%)	1 (14.29%)
400-500	8 (5.30%)	6 (19.35%)	4 (17.39%)	0 (0.00%)
>500	9 (5.96%)	2 (6.45%)	5 (21.74%)	5 (71.43%)

a is Pre-line, b is Post-line, c is Lineament structure map, and d is Geological map [37].

The methodological approach adopted in this study differs from lineament extraction strategies commonly applied in non-tropical or arid karst regions. In arid settings, such as the Moroccan Anti-Atlas or Zagros Mountains, sparse vegetation allows for the direct delineation of fractures and faults using optical satellite imagery (e.g., Landsat or ASTER) due to high bedrock exposure [39]. In contrast, the tropical karst environment of the present study is characterized by dense canopy cover and intense chemical weathering, which obscure direct spectral identification of geological structures. Consequently, this study emphasizes DEM-derived morphometric indicators and L-band SAR data capable of capturing subtle topographic expressions of structural control (e.g., aligned depressions) beneath vegetation, as similarly reported in tropical karst investigations [32].

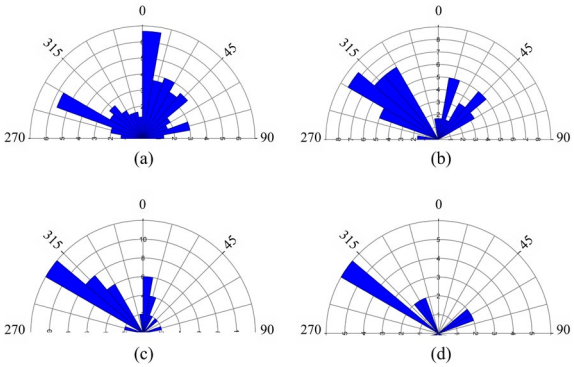

**The rose diagram derived from the geological map was analyzed using the Split Line tool, which resulted in the generation of additional line segments (or sub-lines). Crucially, this segmentation did not affect the directional analysis.*

Fig.5 Rose diagrams illustrating the orientation distribution of lineaments for (a) Pre-line dataset, (b) Post-line dataset, (c) Lineament structure map, and (d) Geological map from DMR [37].

4.4 Karst Depression Analysis

Karst depressions are surface landforms formed through the dissolution of limestone, the same process that generates subsurface caves. Karst depressions and caves originate from the same dissolution processes in carbonate rocks; however, not every surface depression corresponds directly to a mapped cave passage, as subsurface void development is controlled by structural discontinuities and hydraulic pathways that may not produce a clear surface expression. Accordingly, the identification of karst depressions can serve as a diagnostic indicator of potential cave systems in the corresponding area [34, 38].

In this study, karst depressions were identified through differential analysis between filled and unfilled DEMs, a technique inherently based on enforcing hydrologic continuity [40]. The analysis yielded elevation differences ranging from 0 to −6 meters, where negative values suggested potential subsidence or surface depressions. Visually, white areas indicated no change, while black areas represented the deepest depressions. However, as the fill process can alter elevation data to remove imperfections, not all negative values represent genuine karst features. Consequently, the results were rigorously cross-referenced with topographic maps and Sentinel-2 satellite imagery to distinguish true karst depressions from artifacts. This multi-source

verification successfully filtered out non-karstic depressions, isolating three significant depression zones of geological relevance (Fig.6). This integrative approach improved the accuracy of karst feature delineation in complex terrain modeling.

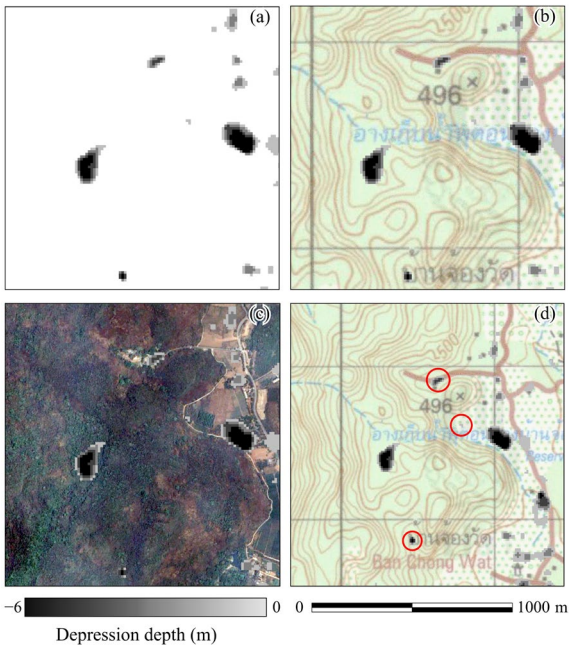

Fig.6 Karst depression analysis showing (a) identified depression areas (DA), (b) DA on the topographic map, (c) DA on Sentinel-2 imagery, and (d) selected area of interest for further evaluation

4.5 Cave Direction Prediction and Validation

The integrated cave direction prediction model utilized a Multiplicative Boolean Overlay within a Map Algebra framework to synthesize four spatial components: Cave Entrance Buffer, High-Density Lineament Zones, Karst Depressions, and Connected fracture lines. The input factors and their specific classification scores are presented in Table 3.

A multiplicative Boolean overlay was selected in preference to weighted linear combination or fuzzy logic approaches because the available validation datasets were insufficient to robustly calibrate continuous weights or membership functions. The objective of this study was to emphasize strict structural coincidence among critical factors rather than allow compensatory effects between variables. In weighted linear models, a high score in one factor may offset the absence of another structurally significant condition. By contrast, the multiplicative scheme restricts high-probability outputs to areas where all favorable structural indicators co-occur, thereby providing a more conservative and structurally constrained prediction consistent with the study objectives.

This methodology successfully generated a probability map classified into five ordinal categories ranging from Very Low to Very High, as illustrated in Fig.7. The predicted high-probability zones predominantly follow a NW-SE structural trend, aligning with the major fracture orientations identified in the region.

Table 3. Factors used in evaluating the probability of the Cave direction.

Parameter	Classification	Factor value
Cave entrance	Absent	1
	Present	2
Karst depression	Absent	1
	Present	2
Lineament density	Very low	1
	Low	2
	Intermediate	3
	High	4
	Very high	5

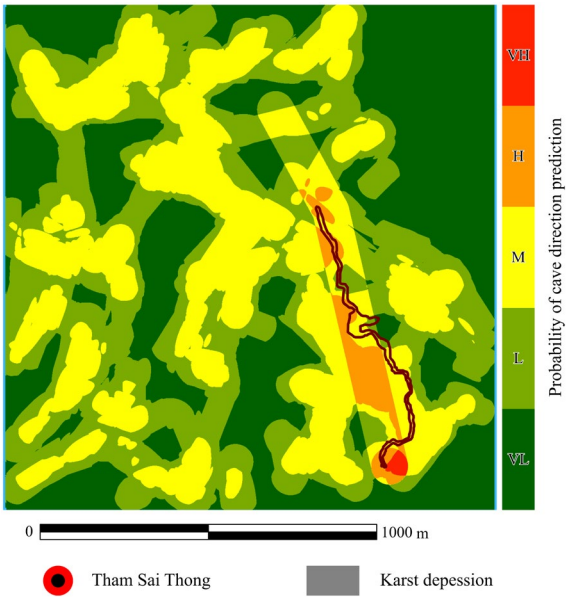

Fig.7 Probability map of cave direction prediction classified into five ordinal categories: Very High (VH), High (H), Moderate or Intermediate (M), Low (L), and Very Low (VL).

It should be emphasized that the extracted lineaments represent surface geomorphic expressions of structural discontinuities and do not directly confirm fracture aperture, sealing condition, or hydraulic transmissivity. In structural terms, such fractures may be sealed by secondary mineralization, mechanically inactive, or hydraulically transmissive and actively conducting groundwater. Because remote sensing-derived lineaments capture surface

morphology rather than subsurface hydraulic properties, the present framework evaluates structural alignment as a proxy for potential subsurface guidance rather than verified fluid-flow pathways.

4.6 Cave Direction Evaluation

The predictive map was validated against two external datasets: the field survey by Ellis [41] and the geological map by Bunchaiwong et al. [23].

4.6.1 Directional Consistency

The predicted NW-SE trend was consistent with the actual mapped cave directions (NW-SE and NNW-SSE), as shown in the comparative rose diagrams (Fig. 8).

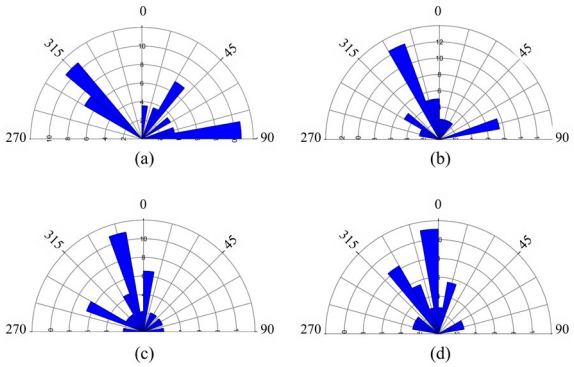

Fig.8 Rose diagrams of structural and cave orientations: (a) lineaments of Tham Sai Thong (this study), (b) cave directions by [41], (c) cave directions, and (d) lineaments from [23].

4.6.2 Spatial Overlap Accuracy

The spatial intersection of the actual mapped cave area with the predicted probability zones (Intermediate to Very High) was calculated. The model achieved an accuracy of 93.67% against the Ellis data [41] and 81.47% against the Bunchaiwong et al. data [23]. The detailed evaluation results are summarized in Table 4 and visualized in Fig. 9.

The accuracy assessment was conducted using vector-based intersection analysis. The cave maps were buffered at 50 m following the Optimum Legible Delineation (OLD) criterion (4 × 12.5 m pixel size) to account for positional tolerance and spatial generalization inherent in both datasets. Overlap percentages were calculated relative to the buffered cave extent. It should be noted that the probability map represents an ordinal susceptibility classification rather than a binary prediction model; therefore, areas categorized as Low or Very Low do not necessarily indicate model error but reflect comparatively lower structural coincidence under the defined criteria.

The present study does not define a single deterministic "correlation length" between individual surface fracture traces and mapped cave passages. Such a parameter would be poorly constrained given the 12.5 m DEM resolution and the absence of detailed subsurface fracture measurements at the scale of individual cave passages. Instead, structural correspondence is interpreted at two complementary scales. At the local scale, spatial coincidence is evaluated within the 50 m OLD-based buffer, representing positional tolerance consistent with the mapping resolution. At the regional scale, correlation is assessed through statistical alignment of dominant orientation modes across hundreds of meters to kilometers. The spatial resolution of the ALOS DEM constrains the minimum size of detectable topographic discontinuities; therefore, subtle meter-scale fractures may not be individually resolved. While higher-resolution LiDAR data would likely refine the delineation of minor fracture traces and karst depressions, it is unlikely to significantly alter the principal structural orientation trends observed at the present mapping scale, as these trends are consistent with independently mapped regional tectonic structures.

These results indicate strong spatial correspondence between predicted moderate-to-high probability zones and confirmed cave extents, supporting the applicability of the semi-automated lineament extraction and multi-criteria spatial overlay approach in structurally controlled karst terrain.

Table 4. Evaluation of the Accuracy of Cave Direction Compared to the Cave Maps by Bunchaiwong et al. and Ellis.

Probability of a cave	Bunchaiwong et al (m^2)	Ellis (m^2)
Very low	141 (1.26%)	0 (0.00%)
Low	1924 (17.27%)	663 (6.33%)
Intermediate	6267 (56.25%)	6320 (60.37%)
High	2809 (25.21%)	3464 (33.09%)
Very high	0 (0.00%)	22 (0.21%)
Evaluation of cave	81.47%	93.67%

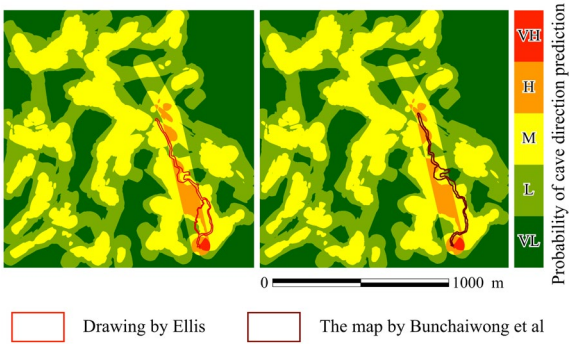

Fig.9 Image showing the layout of the real cave superimposed with the probable cave direction area.

5. CONCLUSION

This study demonstrates that a semi-automated geospatial framework can effectively predict structurally controlled cave directions in the complex tropical karst terrain of Tham Sai Thong, Chiang Rai. The integration of Topographic Position Index (TPI) enhancement with Hough Transform extraction produced structurally coherent lineaments, with the refined "Post-Line" dataset exhibiting an average length of 343.94 m, closely aligned with the 356.00 m average reported in the official DMR Lineament Structure Map [37]. Orientation analysis further identified dominant NW–SE and NNE–SSW trends consistent with the regional tectonic framework, particularly the Mae Chan Fault system.

The integrated Multiplicative Boolean Overlay model, combining lineament density, karst depressions, and cave entrance proximity, achieved strong spatial correspondence with independent speleological surveys, yielding an overlap accuracy of 93.67% under the defined tolerance framework. These results indicate that surface-derived structural alignment can serve as a useful structural proxy for guiding subsurface cave direction prediction in vegetation-covered tropical karst environments.

Nevertheless, several limitations should be acknowledged. The analysis is constrained by the 12.5 m DEM resolution, which may not capture smaller-scale discontinuities. Surface-derived lineaments represent geomorphic expressions and do not directly verify fracture transmissivity. Moreover, the predictive framework operates within a two-dimensional planimetric context and does not explicitly model vertical cave development. Areas predicted as high potential but lacking mapped cave occurrence may reflect incomplete subsurface documentation rather than model inadequacy. Future studies incorporating higher-resolution elevation data and field-based structural measurements may further refine predictive performance. In addition, the framework does not explicitly differentiate between sealed, inactive, and hydraulically active fractures.

6. ACKNOWLEDGMENTS

The authors acknowledge financial and facility support from Suranaree University of Technology (SUT). This research was supported by the "Development Project for Integrating Communication Systems, Positioning Systems, and a Visualization System for Exploring and Mapping Caves," funded by the National Broadcasting and Telecommunications Commission (NBTC). The authors thank Tham Luang–Khun Nam Nang Non National Park, Ministry of Natural Resources and Environment, for facilitating cave exploration, and the Department of Mineral Resources (DMR) for providing geological and structural data.

7. REFERENCES

1. Suttiwaree, P., Putthaprasert, P., Phuthanawiroj, P., Bungnam, M., Aksornthueng, S., and Atthakor, W., Multi-Dimensional Management: A Case Study of Tham Luang Cave Rescue, Journal of Public and Private Management, Vol. 29, No. 1, 2022, pp. 37–57.
2. GISTDA, Study the three-dimensional images of Tham Luang–Khun Nam Nang Non, 2018, available at: https://www.gistda.or.th/main/th/node/2648
3. Uamjaiboon, W., Tham Luang Khun Nam Nang Non Chiang Rai Province: Local learning resources with geological changes, Geotechnical Division, Department of Mineral Resources, Bangkok, 2021.
4. Tansuwan, K., and Ongsomwang, S., Proper edge enhancement of satellite and DEM shaded relief images for visually geologic lineament interpretation in Pha Taem National Park, Thailand, Journal of Remote Sensing and GIS Association of Thailand, Vol. 24, 2023, pp. 18–37.
5. Hobbs, W. H., Lineaments of the Atlantic Border region, GSA Bulletin, Vol. 15, No. 1, 1904, pp. 483–506. https://doi.org/10.1130/GSAB-15-483
6. Hobbs, W. H., Earth features and their meaning: An introduction to geology for the student and the general reader, The Macmillan Company, New York, 1912.
7. Vassilas, N., Perantonis, S., Charou, E., Tsenoglou, T., Stefouli, M., and Varoufakis, S., Delineation of lineaments from satellite data based on efficient neural network and pattern recognition techniques, Proceedings of the 2nd Hellenic Conference on Artificial Intelligence (SETN 2002), 2002, pp. 355–365.
8. Ahmadi, H., and Pekkan, E., Fault-Based Geological Lineaments Extraction Using Remote Sensing and GIS—A Review, Geosciences, Vol. 11, No. 5, 2021, Article 183. https://doi.org/10.3390/geosciences11050183
9. Pardo-Igúzquiza, E., Valsero, J. J. D., and Dowd, P. A., Automatic detection and delineation of karst terrain depressions and its application in geomorphological mapping and morphometric analysis, Acta Carsologica, Vol. 42, No. 1, 2013. https://doi.org/10.3986/ac.v42i1.637
10. Yeomans, C. M., Claridge, H., Hudson, A. J., Shail, R. K., Willems, C., Eyre, M., and Harker, C., A single multi-scale and multi-sourced semi-automated lineament detection technique for detailed structural mapping with applications to geothermal energy exploration, Quarterly Journal of Engineering Geology and Hydrogeology, Vol. 56, No. 2, 2023, Article qjegh2022-051. https://doi.org/10.1144/qjegh2022-051

11. Sadeghi, S., Teshnizi, E. S., Pash, R. R., and Golian, M., Extraction of Lineaments Using Landsat Image and Digital Elevation Model: A Case Study of Zagros Orogenic Belt, West Iran, Journal of the Indian Society of Remote Sensing, Vol. 52, No. 11, 2024, pp. 2361–2373. https://doi.org/10.1007/s12524-024-01956-5
12. Chakouri, M., Jellouli, A., Hajaj, S., El Hachimi, J., Ouguinaz, A., Aangri, A., and El Harti, A., Comparative analysis of SAR sensors for effective tectonic lineament mapping in semiarid region, E3S Web of Conferences, Vol. 607, 2025, Article 01002. https://doi.org/10.1051/e3sconf/202560701002
13. Opara, J. N., Moriwaki, R., and Chun, P. J., Ensemble Learning-Based Automatic Detection of Landslide Areas from Aerial Photographs, International Journal of GEOMATE, Vol. 27, No. 122, 2024. https://doi.org/10.21660/2024.122.g13142
14. Manyoe, I. N., and Hutagalung, R., The extraction and analysis of lineament density from digital elevation model in Libungo geothermal area, Gorontalo, IOP Conference Series: Earth and Environmental Science, Vol. 1089, No. 1, 2022, Article 012012. https://doi.org/10.1088/1755-315/1089/1/012012
15. Suasti, Y., Caesario, D., Prihantarto, W. J., Susetyo, B. B., and Iskarni, P., Development of Active Fault Mapping Method Using Geoelectric and Geographical Information System, International Journal of GEOMATE, Vol. 26, No. 116, 2024, pp. 72–84. https://doi.org/10.21660/2024.116.4360
16. Jiang, G., Chen, Z., Siripornpibul, C., Haryono, E., Nguyen, N. X., Oo, T., and Guo, F., The karst water environment in Southeast Asia: Characteristics, challenges, and approaches, Hydrogeology Journal, Vol. 29, No. 1, 2021, pp. 123–135. https://doi.org/10.1007/s10040-020-02267-y
17. El-Haddad, B. A., Youssef, A. M., El-Shater, A. H., and El-Khashab, M. H., Geohazards related to karst and slope instability along the Safaga–Gabal El-Zeit area, Red Sea Coast, Egypt, Sohag Journal of Sciences, Vol. 7, No. 2, 2022, pp. 37–45. https://doi.org/10.21608/sjsci.2022.233684
18. Purwaningsih, E., Liusti, S. A., Purnamasari, E., Ramadhan, R., and Nasution, A. F. R., The Mount Marapi eruption disaster evacuation path model using a local wisdom approach, International Journal of GEOMATE, Vol. 26, No. 116, 2024, pp. 64–71. https://doi.org/10.21660/2024.116.4353
19. Duan, L., Lim, H. S., Sharoni, S. R. M. H. M., Chen, M., Han, N., and Tian, X., Assessing highway slope stability risks using InSAR: A case study in Bijie, China, Geocarto International, Vol. 40, No. 1, 2025, pp. 1-22. https://doi.org/10.1080/10106049.2025.2521661
20. Le Corre, D., Mason, N., Bernard-Salas, J., Mary, D., and Cox, N., New candidate cave entrances on the Moon found using deep learning, Icarus, Vol. 441, 2025, Article 116675. https://doi.org/10.1016/j.icarus.2025.116675
21. Qin, Z., Zhang, Q., Yu, S., Yang, Y., Zhang, J., Xu, M., Liu, Y., Liu, M., and Nie, M., Revealing karst water circulation based on GIS and environmental isotopes methods—A case study in eastern Sichuan, southwestern China, Frontiers in Earth Science, Vol. 11, 2023. https://doi.org/10.3389/feart.2023.1120618
22. The Royal Thai Survey Department, Topographic map of Mae Sai District, Thailand, scale 1:50,000, sheet 4949 I, series L7018, edition 2-RTSD, Bangkok, 1999.
23. Bunchaiwong, N., Duangkhamsawat, J., Chanfu, N., Maneekiang, N., and Khamcha, C., A report on the survey and research of the Tham Sai Thong Cave System–Khun Nam Nang Non Cave, Geotechnical Division, Department of Mineral Resources, Bangkok, 2022.
24. Copernicus Open Access Hub, Sentinel-2 S2A, 2024, available at: https://scihub.copernicus.eu/
25. Alaska Satellite Facility, ALOS PALSAR - Radiometric Terrain Correction, ASF DAAC, 2015, https://doi.org/10.5067/Z97HFCNKR6VA.
26. Echeverria, M. D. P. V., Ortega, A. G. V., Larreta, E., Crespo, P. R., and Mulas, M., Lineament extraction from digital terrain derivative model: A case study in the Girón–Santa Isabel Basin, South Ecuador, Remote Sensing, Vol. 14, No. 21, 2022, Article 5400. https://doi.org/10.3390/rs14215400
27. Gonzalez, R. C., and Woods, R. E., Digital Image Processing, 4th ed., Pearson Education, New York, 2018.
28. Duda, R. O., and Hart, P. E., Use of the Hough transformation to detect lines and curves in pictures, Communications of the ACM, Vol. 15, No. 1, 1972, pp. 11–15. https://doi.org/10.1145/361237.361242
29. Sander, P., Minor, T. B., and Chesley, M. M., Groundwater exploration based on lineament analysis and reproducibility testing, Groundwater, Vol. 35, No. 5, 1997, pp. 888–894. https://doi.org/10.1111/j.1745-6584.1997.tb00157.x

30. Kalbasi, M., and Nikmehr, H., Noise-robust, reconfigurable Canny edge detection and its hardware realization, IEEE Access, Vol. 8, 2020, pp. 39934–39945. https://doi.org/10.1109/ACCESS.2020.2976860
31. Asano, T., Algorithmic evaluation of line detection problem, Interdisciplinary Information Sciences, Vol. 8, No. 2, 2002, pp. 137–145. https://doi.org/10.4036/iis.2002.137
32. Hung, L. Q., Dinh, N. Q., Batelaan, O., Tam, V. T., and Lagrou, D., Remote sensing and GIS-based analysis of cave development in the Suoimuoi catchment (Son La–NW Vietnam), Journal of Cave and Karst Studies, Vol. 64, No. 1, 2002, pp. 23–33.
33. Vink, A. P. A., Land use in advancing agriculture, Springer-Verlag, 1975.
34. Ford, D., and Williams, P., Karst Hydrogeology and Geomorphology, Wiley, Chichester, 2007. https://doi.org/10.1002/9781118684986
35. Jenks, G. F., The data model concept in statistical mapping, International Yearbook of Cartography, Vol. 7, 1967, pp. 186–190.
36. Slocum, T. A., McMaster, R. B., Kessler, F. C., and Howard, H. H., Thematic Cartography and Geovisualization, 3rd ed., Prentice Hall, Upper Saddle River, 2009.
37. Department of Mineral Resources (DMR), Final report on the geological and hydrogeological survey project of the limestone mountain range in Tham Luang Khun Nam Nang Non National Park, Geotechnical Division, Department of Mineral Resources, Bangkok, 2021.
38. White, W. B., Geomorphology and Hydrology of Karst Terrains, Oxford University Press, 1988.
39. Adiri, Z., El Harti, A., Jellouli, A., Maacha, L., and Bachaoui, E. M., Comparison of Landsat-8, ASTER and Sentinel-1 satellite remote sensing data in automatic lineaments extraction: A case study of Sidi Flah–Bouskour inlier, Moroccan Anti-Atlas, Advances in Space Research, Vol. 60, No. 11, 2017, pp. 2355–2367. https://doi.org/10.1016/j.asr.2017.09.006
40. Planchon, O., and Darboux, F., A fast, simple and versatile algorithm to fill the depressions of digital elevation models, Catena, Vol. 46, No. 2–3, 2001, pp. 159–176. https://doi.org/10.1016/s0341-8162(01)00164-3
41. Ellis, M., The cave of Tham Luang Khun Nam Nang Non National Park, Shepton Mallet Caving Club Reports, 2023.